

A Model of the Heliosphere with Jets

J. F. Drake¹, M. Swisdak¹, M. Opher²

ABSTRACT

An analytic model of the heliosheath (HS) between the termination shock (TS) and the heliopause (HP) is developed in the limit in which the interstellar flow and magnetic field are neglected. The heliosphere in this limit is axisymmetric and the overall structure of the HS and HP are controlled by the solar magnetic field even in the limit in which the ratio of the plasma to magnetic field pressure, $\beta = 8\pi P/B^2$, in the HS is large. The tension of the solar magnetic field produces a drop in the total pressure between the TS and the HP. This same pressure drop accelerates the plasma flow downstream of the TS into the North and South directions to form two collimated jets. The radii of these jets are controlled by the flow through the TS and the acceleration of this flow by the magnetic field – a stronger solar magnetic field boosts the velocity of the jets and reduces the radii of the jets and the HP. Magnetohydrodynamic (MHD) simulations of the global heliosphere embedded in a stationary interstellar medium match well with the analytic model. The results suggest that mechanisms that reduce the HS plasma pressure downstream of the TS can enhance the jet outflow velocity and reduce the HP radius to values more consistent with the Voyager 1 observations than in current global models.

Subject headings: ISM: jets and outflows – Stars: jets – Sun: heliosphere – Sun: magnetic fields

1. INTRODUCTION

The historically accepted shape of the heliosphere is that of a comet-like object with a long tail that is dragged downstream by the flow of the local interstellar medium (LISM) past the sun (Parker 1961; Baranov & Malama 1993). These early pictures, however, were based on a hydrodynamic description of the solar outflow – the solar magnetic field was assumed to

¹University of Maryland, College Park, MD, USA; drake@umd.edu, swisdak@umd.edu

²Astronomy Department, Boston University, Boston, MA, USA ; mopher@bu.edu

play a negligible role in the overall structure of the heliosphere and its interaction with the solar wind. Computational models based on the magnetohydrodynamic (MHD) equations included the solar magnetic field as well as that of the interstellar medium and also produced a heliosphere with a comet-like shape (Opher et al. 2006; Pogorelov et al. 2007; Opher et al. 2009; Washimi et al. 2011; Pogorelov et al. 2013; Opher & Drake 2013).

On the other hand, the measurements of energetic neutral atoms (ENAs) by IBEX and CASSINI produced some surprises. These ENAs travel long distances through the heliosphere without being influenced by the ambient magnetic field and therefore yield information about the large-scale structure of the heliosphere. The CASSINI ENA fluxes from the direction of the nose and the tail were comparable, leading the CASSINI observers to conclude that the heliosphere was “tailless” (Krimigis et al. 2009; Dialynas et al. 2013). The IBEX observations from the tail revealed that the hardest spectrum of ENAs were localized in two lobes at high latitude while the softest spectra were at low latitudes (McComas et al. 2013).

Recent MHD simulations using a monopole model for the solar magnetic field, designed to reduce the numerical dissipation of magnetic energy that arises from a conventional dipole model, revealed that the solar magnetic field was strong enough to collimate the solar wind into a pair of jets that flow to the North and South (Opher et al. 2015). These jets bend in the direction of the tail, pushed by the flow of the LISM. The interstellar rather than the solar wind plasma flows between these jets in the equatorial region downstream. Such bent jets have been seen in protostellar systems (Fendt & Zinnecker 1998; Gueth & Guilloteau 1999) and clusters of galaxies (Owen & Rudnick 1976). Astrophysical jets around massive black holes are thought to be driven by centrifugal forces that sling the plasma along a rotating helical magnetic field (Blandford & Payne 1982). However, the jets in the case of the heliosphere are driven in the region downstream of the TS as was proposed for the Crab Nebula (Begelman & Li 1992; Chevalier & Luo 1994; Lyubarsky 2002). In this region of subsonic flow, the magnetic tension (hoop) force is strong enough to collimate and drive the wind.

MHD models of the global heliosphere are complex and the mechanisms that control the shape of the HP, the thickness of the HS, the structure of the heliospheric jets, including the driver for the outflow, remain uncertain. The Voyager 1 observations have revealed that the thickness of the HS is around $30AU$, which is substantially thinner than expected from the global simulations. We present an analytic model of the heliosphere outside of a spherically symmetric TS where we neglect the ambient flow and magnetic field of the LISM. Taking the resulting heliosphere as axisymmetric and the flows within the HS as subsonic, we obtain the pressure and magnetic field structure of the HS along with the radius r_{hp} of the HP.

The overall shape of the HS takes the classic form of an astrophysical jet: the flows through the TS are accelerated to the North and South by the solar magnetic field. The heliopause radius is determined by continuity: the plasma flow through the TS must balance the outflow through the jets. We present parallel global MHD simulations in the limit of zero magnetic field and flow in the LISM which support the analytic model.

One reason the influence of the solar magnetic field on the structure of the heliosphere is often neglected in the literature is because the pressure of the ambient plasma is large compared with that of the magnetic field – $\beta = 8\pi nT/B^2 \sim 10$ just downstream of the TS. We show, however, that the total plasma pressure does not control either the flows in or the thickness of the HS. The overall pressure in the HS is balanced by the pressure in the LISM. It is the tension force of the HS magnetic field that controls the pressure difference between the TS and HP (Axford 1972). To the North and South there is no tension force and this same pressure difference drives the axial flow of the heliospheric jets. Thus, it is ultimately the solar magnetic field that controls the large-scale structure of the HS.

2. Analytic Model of the Heliosheath and Heliopause

We consider a simple axisymmetric system in which there is no LISM flow or magnetic field and the LISM is specified by its ambient pressure P_{LISM} . We write down the steady-state MHD equations, including continuity, pressure, momentum and magnetic field,

$$\nabla \cdot n\mathbf{V} = 0, \quad (1)$$

$$\nabla \cdot P^{1/\Gamma}\mathbf{V} = 0, \quad (2)$$

$$M\nabla \cdot n\mathbf{V}\mathbf{V} = -\nabla \left(P + \frac{B^2}{8\pi} \right) - \frac{B^2}{4\pi r} \nabla r, \quad (3)$$

$$\nabla \times (\mathbf{V} \times \mathbf{B}) = 0, \quad (4)$$

where r is the radius in cylindrical coordinates, Γ is the ratio of specific heats and \mathbf{B} is in the azimuthal direction. These equations are solved in the HS with boundary conditions on the density, pressure, magnetic field and flow given just downstream of the spherical TS which has a spherical coordinate radius R_s . At the TS we assume that the azimuth flow V_ϕ is zero and since there are no forces in the ϕ direction (Eq. (3)), we can take $V_\phi = 0$ everywhere. Thus, from Eq. (1) we can write

$$n\mathbf{V} = \nabla\phi \times \nabla\psi, \quad (5)$$

where ψ is the stream function for the particle flux. Taking $\mathbf{B} = rB\nabla\phi$ with \mathbf{V} from Eq. (5), we can reform Faraday’s law in Eq. (4) as

$$\nabla\psi \times \nabla\left(\frac{B}{nr}\right) = 0. \quad (6)$$

This equation has components only in the ϕ direction so taking the dot product of this equation with $\nabla\phi$ yields the constraint that B/nr is constant along streamlines or

$$B/nr = f(\psi), \quad (7)$$

where the function f is only a function of ψ . The form of f can be determined by the boundary conditions along the TS. Downstream of the TS we take the flow to be normal to the shock, in the radial (in spherical coordinates) direction with a constant value V_s with the density n_s also constant. So, from Eq. (5) we find $\partial\psi/\partial\theta = -R_s^2 n_s V_s \sin\theta$ or

$$\psi = n_s V_s R_s^2 \cos\theta_s, \quad (8)$$

where θ_s is the polar angle in spherical coordinates at the shock. Thus, the variation of ψ along the shock is known. Similarly, we know from the solutions of the Parker spiral magnetic field that along the shock $B = B_s \sin\theta_s$ so $B/nr = B_s/n_s R_s$ is a constant and so is $f = B_s/n_s R_s$. Throughout the HS we have

$$\frac{B}{nr} = \frac{B_s}{n_s R_s}. \quad (9)$$

Turning to the pressure equation and using Eq. (5), we find $\nabla\phi \times \nabla\psi \cdot \nabla(P/(n^\Gamma)) = 0$ so P/n^Γ is also constant along a streamline and therefore a function only of ψ . As before, we can evaluate it along the TS where it is given by P_0/n_s^Γ . Thus,

$$P = P_s \left(\frac{n}{n_s}\right)^\Gamma = P_s \left(\frac{BR_s}{B_s r}\right)^\Gamma. \quad (10)$$

Thus, both P and n in the HS are linked to B and r .

We now focus on the high β limit, which is most relevant to the HS, where the pressure associated with interstellar pickup ions dominates the magnetic pressure. Specifically, we take β to be a large parameter. In addition, since the flows are subsonic downstream of the TS, inertial forces are also small. We can therefore write the plasma pressure in a series $P_0 + P_1 + \dots$ with $P_1 \sim B^2/8\pi \sim MnV^2/2 \ll P_0$. Thus, to lowest order Eq. (3) becomes

$$0 = -\nabla P_0(B, r), \quad (11)$$

where P_0 is an explicit function of B and r through Eq. (10). Equation (10) requires that to lowest order the pressure in the HS is constant everywhere and is given the value P_s at the TS. The density is also a constant, n_s . Since P is linked to B and r through Eq. (10) the constancy of P_0 requires that

$$B = B_s \frac{r}{R_s} \quad (12)$$

so that B increases with radius outside of the TS (Axford 1972; Chevalier & Luo 1994). At first order we include the inertial terms and magnetic field in the momentum equation, which becomes

$$Mn_s \mathbf{V}_0 \cdot \nabla \mathbf{V}_0 = -\nabla \left(P_1 + \frac{B_s^2 r^2}{8\pi R_s^2} \right) - \frac{B_s^2 r}{4\pi R_s^2} \nabla r, \quad (13)$$

where n has been replaced by n_s and $\mathbf{V}_0 = \nabla \phi \times \nabla \psi / n_s$.

Before discussing the flows in the HS, we consider the weak flow limit of Eq. (13) so that the inertial forces in the radial direction can be discarded. In this limit the magnetic tension force in Eq. (13) causes the plasma pressure and total pressure to decrease with radius. This limit is artificial for the HS since the flow V_s downstream of the TS is comparable to the Alfvén speed and the associated radial inertial forces are comparable to the magnetic forces. Nevertheless, this limit illustrates how the pressure in the HS varies. We do not require zero pressure gradient in z . The pressure drop from the TS to the LISM is balanced by magnetic tension in the radial direction but the same pressure drop also develops from the equator to the outflow jets to the North and South. This pressure gradient along z drives the outward flows associated with the jets. Thus, we integrate Eq. (13) from the TS outwards to obtain an explicit expression for P_1 ,

$$P_1(r) = -\frac{B_s^2}{4\pi R_s^2} (r^2 - R_s^2 \sin^2 \theta_s), \quad (14)$$

where $\theta_s(z)$ is the value of θ at the TS and is dependent on z . Pressure balance across the HP, which requires that $P(r_{hp}) + B^2(r_{hp})/8\pi = P_{LISM}$, then yields an explicit expression for r_{hp} ,

$$\frac{r_{hp}^2}{R_s^2} = \frac{8\pi \Delta P}{B_s^2} + 2 \sin^2 \theta_s, \quad (15)$$

where $\Delta P = P_s - P_{LISM}$. At this stage in the calculation the pressure difference ΔP remains undetermined. We will show, however, that the requirement that the mass flow into the HS across the TS balance that out the two jets constrains the pressure difference. In Fig. 1 we show 2-D plots of the plasma pressure, the magnetic pressure and the total pressure in the r, z plane in the HS. The data is shown for $8\pi \Delta P / B_s^2 = 2$, which as shown later is the upper limit on ΔP . The inner boundary of the data shown is the TS and the outer boundary is the HP. The radius of the HP peaks at the midplane and falls off with z until $z > R_s$, where

it remains constant, forming the Northward jet. The plasma and total pressure decrease with radius r while the magnetic pressure increases with r . The total pressure falls off with distance from the equator until it approaches a constant value in the jet. We will show that this pressure difference, which is a consequence of magnetic tension, drives the jet outflow. Along the axis P remains constant at P_s . This shape was obtained by neglecting the radial plasma inertia, an assumption which breaks down where the straight portion of the HP in Fig. 1 intersects the curved portion at $z/R_s = 1$. The sharp kink in the HP is not real and is not seen in the MHD simulations discussed later. In Fig. 2 cuts along r of the total, plasma and magnetic pressures from the data of Fig. 1 are shown at the equator in (a) and across the jet in (b).

We now discuss the flows driven in the HS. We derive a Bernoulli-like equation by taking the dot product of Eq. (13) with \mathbf{V}_0 and integrating along the streamline,

$$\frac{1}{2}Mn_sV_0^2 + P_1 + \frac{B_s^2r^2}{4\pi R_s^2} = \frac{1}{2}Mn_sV_s^2 + \frac{B_s^2\sin^2\theta_s}{4\pi}. \quad (16)$$

Unfortunately, this equation does not enable us to calculate V_0 throughout the HS because it requires that we know the trajectory of a stream line within the HS to link the local radius r with its position at the TS where θ_s is known. Along the axis where $\theta_s = 0$ Eq. (16) gives $V_0 = V_s$, since the pressure is constant and B is zero. Similarly, the velocity at the jet radius r_{jet} , can be calculated since at that location $\theta_s = \pi/2$. We find $V_0^2(r_{jet}) = V_s^2 + c_{As}^2$, where $c_{As}^2 = B_s^2/4\pi Mn_s$. Thus, the increase in the jet velocity above V_s is linked to the Alfvén velocity based on the magnetic field strength B_s at the TS. More generally, we can calculate $V_0(r)$ across the jet radius by noting that within the jet

$$V_0 = V_{0z} = -\frac{1}{n_sr} \frac{\partial\psi}{\partial r}. \quad (17)$$

From Eq. (8) $\sin\theta_s$ can be written in terms of ψ so we are left with a single equation for ψ across the jet,

$$\frac{1}{n_s^2r^2} \left(\frac{\partial\psi}{\partial r} \right)^2 = V_s^2 + 2c_{As}^2 \left(1 - \frac{\psi^2}{n_s^2R_s^4V_s^2} \right), \quad (18)$$

where ψ varies from $n_sV_sR_s^2$ at the jet axis to 0 at the HP. The equality of the particle fluxes through the TS and jets requires that Eq. (18) produce the requisite jump in ψ across the jet. Equation (18) can be simplified by defining an angle variable $\cos\theta = \psi/n_sV_sn_s^2$,

$$\frac{R_s^4\sin^2\theta}{r^2} \left(\frac{\partial\theta}{\partial r} \right)^2 = 1 + 2\frac{c_{As}^2}{V_s^2} \sin^2\theta, \quad (19)$$

where θ varies from 0 at the jet axis to $\pi/2$ at the HP. This equation can be integrated

directly to obtain the jet radius r_{jet} ,

$$r_{jet}^2 = 2R_s^2 \frac{\tan^{-1}(\sqrt{2}c_{As}/V_s)}{\sqrt{2}c_{As}/V_s} \quad (20)$$

The jet radius is a maximum for $c_{As} \ll V_s$ when the jet outflow velocity is given by V_s . In this limit the conservation of particle flux reduces to the jet cross-sectional area being equal to the TS area or $r_{jet} = \sqrt{2}R_s$. With increasing c_{As} the outflow velocity of the jet increases and r_{jet} decreases. For $c_{As} \gg V_s$, $r_{jet} \propto R_s \sqrt{V_s/c_{As}}$. An expression for the pressure jump ΔP between the TS and the LISM can be calculated from Eq. (15), which is exact in the jet where $V_{0r} = 0$,

$$\Delta P = 2 \frac{B_s^2}{8\pi} \frac{\tan^{-1}(\sqrt{2}c_{As}/V_s)}{\sqrt{2}c_{As}/V_s}. \quad (21)$$

The pressure jump is a maximum when c_{As} is small and decreases with increasing c_{As} . The dependence of r_{jet} and ΔP are shown as functions of c_{As}/V_s in Fig. 3. From Eq. (15) r_{hp} therefore also decreases with increasing c_{As}/V_s .

3. Global MHD Simulations

We have carried out MHD simulations of the global heliosphere without an interstellar wind and magnetic field. Our model is based on the 3D multi-fluid MHD code BATS-R-US. It involves one ionized and four neutral H species as well as the magnetic field of the sun. We used a monopole configuration for the solar magnetic field to eliminate artificial reconnection across the heliospheric current sheet. The basic parameters of the simulation are the same as those described in Opher *et al.* 2015. The computational grid was $\pm 3000 AU$ in each direction. Parameters of the solar wind at the inner boundary at $30 AU$ were: $v_{SW} = 417 km/s$, $n_{SW} = 8.74 \times 10^{-3} cm^{-3}$, $T_{SW} = 1.087 \times 10^5 K$ and the Parker spiral magnetic field with a radial component $B_{SW} = 7.17 \times 10^{-3} nT$ at the equator (with an azimuthal component $B_\phi = 0.22 nT$). The solar wind flow at the inner boundary is assumed to be spherically symmetric and the magnetic axis is aligned with the solar rotation axis. For the LISM we assume $T_{ISM} = 6519 K$ while the plasma density was raised to $0.483/cm^3$ to make up for the absence of pressure associated with the interstellar magnetic field. The number density of H atoms in the interstellar medium is $n_H = 0.18 cm^{-3}$ and the temperature is the same as for the interstellar plasma. The z-axis is parallel to the solar rotation axis. The grid has cells ranging from $2.93 AU$ at the inner boundary to $187.5 AU$ at the outer boundary. The simulation had a resolution of $3.0 AU$ between $z = \pm 750 AU$ and $x = \pm 305 AU$; $y = \pm 400 AU$, encompassing the entire HS. The run was stepped forward for 3061 years.

In Fig. 4 we show in yellow the surface of the HP as defined by $\ln T = 13.9$. The simulation reveals jets to the North and South as in the analytic model. The HP bulges at the equator as in the model. The gray lines are the solar magnetic field. Shown in Fig. 5 in the $x-z$ plane are the plasma pressure in (a), the magnetic pressure in (b) and the speed and streamlines in (c). As in the model, the plasma pressure decreases with cylindrical radius r away from the jet axis while the magnetic pressure increases with r and the strongest magnetic fields are in the equatorial region just upstream of the HP. The streamlines reveal the North and South directed outflows that make up the jets. The HP boundary does not reveal the sharp indentation seen in the model. Finally, in Fig. 2(c) we show cuts of the total pressure (solid), the plasma pressure (dotted), the magnetic pressure (dashed) and the magnetic field (dot-dashed) in cuts along r at the equator from just upstream of the TS to past the HP. The pressures have been normalized to $B_s^2/8\pi$, B to B_s and r to R_s with $R_s = 135AU$ taken to be the location of the maximum of P_{plasma} . The cuts are in remarkable agreement with the cuts from the model in (a). In the simulation $c_{As}/V_s = 1.1$, which from Fig. 3, yields $8\pi\Delta P/B_s^2 = 1.3$ compared with the measured value of 1.5 from Fig. 2(c). For $8\pi\Delta P/B_s^2 = 1.5$ Eq. (15) yields $r_{hp}/R_s = 1.9$ at the equator, essentially identical to the HP radius in the cuts, and the ratio of the HP radius at the equator to that in the jet is 0.64 (Eq. (15)) compared with the measured value of 0.66. Finally the measured particle flux through the TS is the same as that out the jets.

4. Discussion and Conclusions

We have explored the structure of the HS and HP when the interstellar flow and magnetic field are neglected and the system can be treated as axisymmetric. We show that even in the limit in which $P \gg B^2/8\pi$ in the HS the magnetic field controls the large-scale structure of the HS and drives Northward and Southward directed jets. To lowest order the pressure in the HS is balanced by the pressure in the interstellar medium. The magnetic field controls the pressure variation within the HS and re-directs and boosts the flow across the TS to the North and South to form heliospheric jets. The radial distance from the TS to the HP and the jet radii are controlled by the requirement that the plasma flowing into the HS across the TS flows outwards in the jets (see also Yu (1974)). For very weak magnetic fields the jet outflow velocity is the same as the velocity V_s downstream of the TS. In this limit the total cross-sectional area of the jets is equal to the area of the TS and $r_{jet} = \sqrt{2}R_s$. With increasing magnetic field strength the jet outflow velocity increases and the radii of the HP and the outflow jet decrease (Eq. (20) and Fig. 3(a).

The global MHD models of the heliosphere (Malama et al. 2006; Pogorelov et al. 2007;

Opher et al. 2009) produce HS thicknesses that are around $50 - 70AU$, substantially larger than the value of $30AU$ determined from Voyager 1’s crossing of the HP in 2012 (Stone et al. 2013). The results here suggest that mechanisms that increase the jet outflows will reduce the HP radius. Pressure reductions in the downstream region associated with thermal conduction or other mechanisms might produce such enhanced flows.

There is evidence from both the present MHD simulations and those carried out the earlier (Opher et al. 2015) that the jets are subject to large-scale instabilities. The resulting turbulence might be a driver of anomalous cosmic rays (Stone et al. 2005, 2008). High time-resolution ENA measurements might be able to establish the existence of the heliospheric jets and associated turbulence. For a jet radius of around $140AU$ and an Alfvén velocity of around $100km/s$, the Alfvén transit time is around 10 years. The jet turbulence might, of course, cascade to smaller scales so the relevant time scales could be shorter.

This work has been supported by NASA Grand Challenge NNX14AIB0G and NASA awards NNX14AF42G, NNX13AE04G and NNX13AE04G. The MHD simulations were carried out on Pleades at the NASA Ames Research Center under the award SMD-14-4986. We acknowledge support from the International Space Science Institute for the team “Facing the Most Pressing Challenges to Our Understanding of the Heliosheath and its Outer Boundaries.”

REFERENCES

- Axford, W. I. 1972, NASA Special Publication, 308, 609
- Baranov, V. B., & Malama, Y. G. 1993, J. Geophys. Res., 98, 15157
- Begelman, M. C., & Li, Z.-Y. 1992, ApJ, 397, 187
- Blandford, R. D., & Payne, D. G. 1982, Mon. Not. R. Astron. Soc., 199, 883
- Chevalier, R. A., & Luo, D. 1994, ApJ, 421, 225
- Dialynas, K., Krimigis, S. M., Mitchell, D. G., Roelof, E. C., & Decker, R. B. 2013, ApJ, 778, 40
- Fendt, C., & Zinnecker, H. 1998, A&A, 334, 750
- Gueth, F., & Guilloteau, S. 1999, A&A, 343, 571

- Krimigis, S. M., Mitchell, D. G., Roelof, E. C., Hsieh, K. C., & McComas, D. J. 2009, *Science*, 326, 971
- Lyubarsky, Y. E. 2002, *MNRAS*, 329, L34
- Malama, Y. G., Izmodenov, V. V., & Chalov, S. V. 2006, *A&A*, 445, 693
- McComas, D. J., Dayeh, M. A., Funsten, H. O., Livadiotis, G., & Schwadron, N. A. 2013, *ApJ*, 771, 77
- Opher, M., & Drake, J. F. 2013, *ApJ Lett.*, 778, L26
- Opher, M., Drake, J. F., Zieger, B., & Gombosi, T. I. 2015, *ApJ Lett.*, 800, L28
- Opher, M., Richardson, J. C., Toth, G., & Gombosi, T. I. 2009, *Space Sci. Rev.*, 143, 43
- Opher, M., Stone, E. C., & Liewer, P. C. 2006, *ApJ*, 640, L71
- Owen, F. N., & Rudnick, L. 1976, *ApJ Lett.*, 205, L1
- Parker, E. N. 1961, *ApJ*, 134, 20
- Pogorelov, N. V., Stone, E. C., Florinski, V., & Zank, G. P. 2007, *ApJ*, 668, 611
- Pogorelov, N. V., Suess, S. T., Borovikov, S. N., Ebert, R. W., McComas, D. J., & Zank, G. P. 2013, *ApJ*, 772, 2
- Stone, E. C., Cummings, A. C., McDonald, F. B., Heikkila, B. C., Lal, N., & Webber, W. R. 2005, *Science*, 309, 2017
- . 2008, *Nature*, 454, 71
- Stone, E. C., Cummings, A. C., McDonald, F. B., Heikkila, B. C., Lal, N., & Webber, W. R. 2013, *Science*, 341, 150
- Washimi, H., Zank, G. P., Hu, Q., Tanaka, T., Munakata, K., & Shinagawa, H. 2011, *Mon. Not. R. Astron. Soc.*, 416, 1475
- Yu, G. 1974, *ApJ*, 194, 187

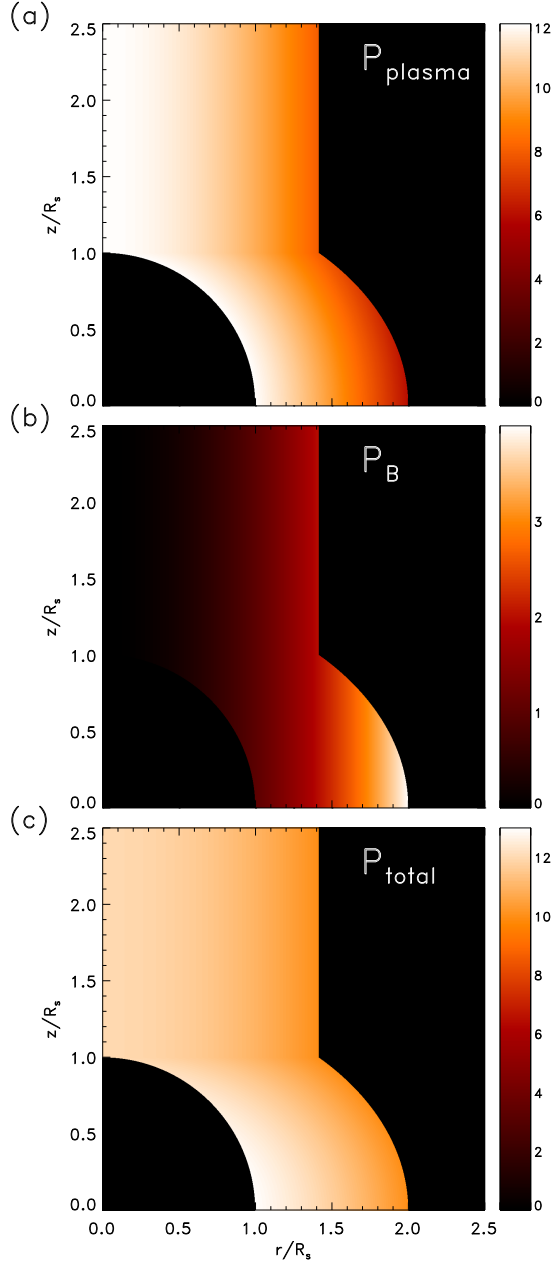


Fig. 1.— 2-D images in the HS of the plasma pressure in (a), the magnetic pressure in (b) and the total pressure in (c), all normalized to $P_{Bs} = B_s^2/8\pi$, where B_s is the magnetic field just downstream of the TS at the equator. The images are for $\Delta P = P_s - P_{LISM} = 2B_s^2/8\pi$ and $\beta_s = P_s/P_{Bs} = 12$, where P_s is the plasma pressure downstream of the TS and P_{LISM} is the pressure of the LISM.

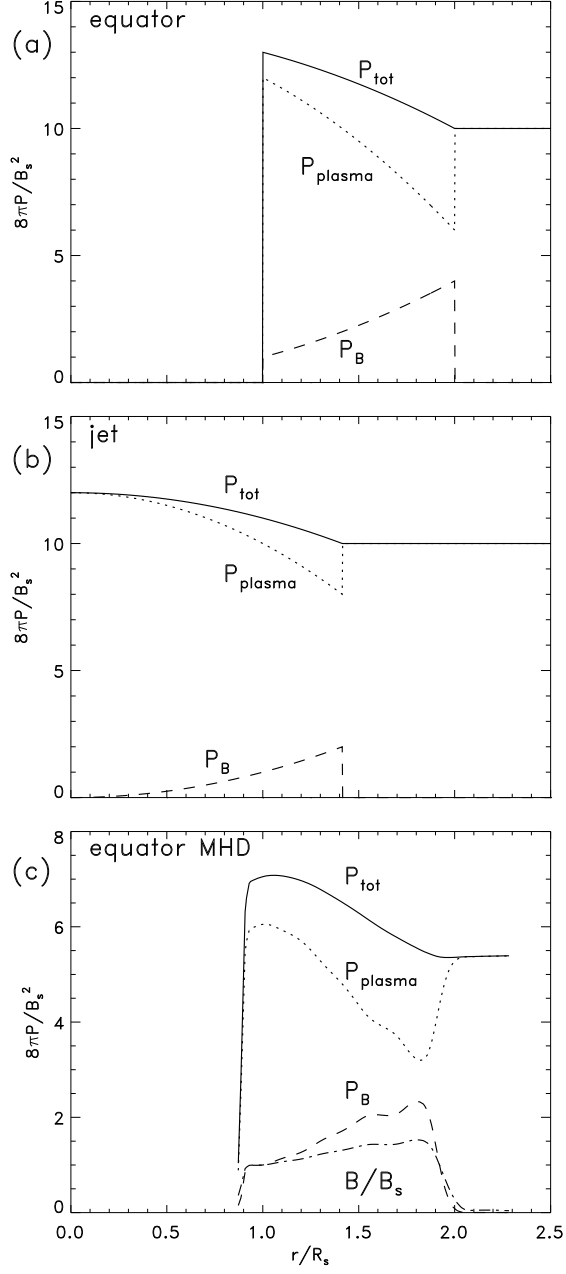


Fig. 2.— Cuts through the data of Fig. 1 of the total pressure (solid), plasma pressure (dotted) and magnetic pressure (dashed) versus r at the equator in (a) and within the jet in (b). In (c) cuts from the MHD simulation of Fig. 4 along the equator.

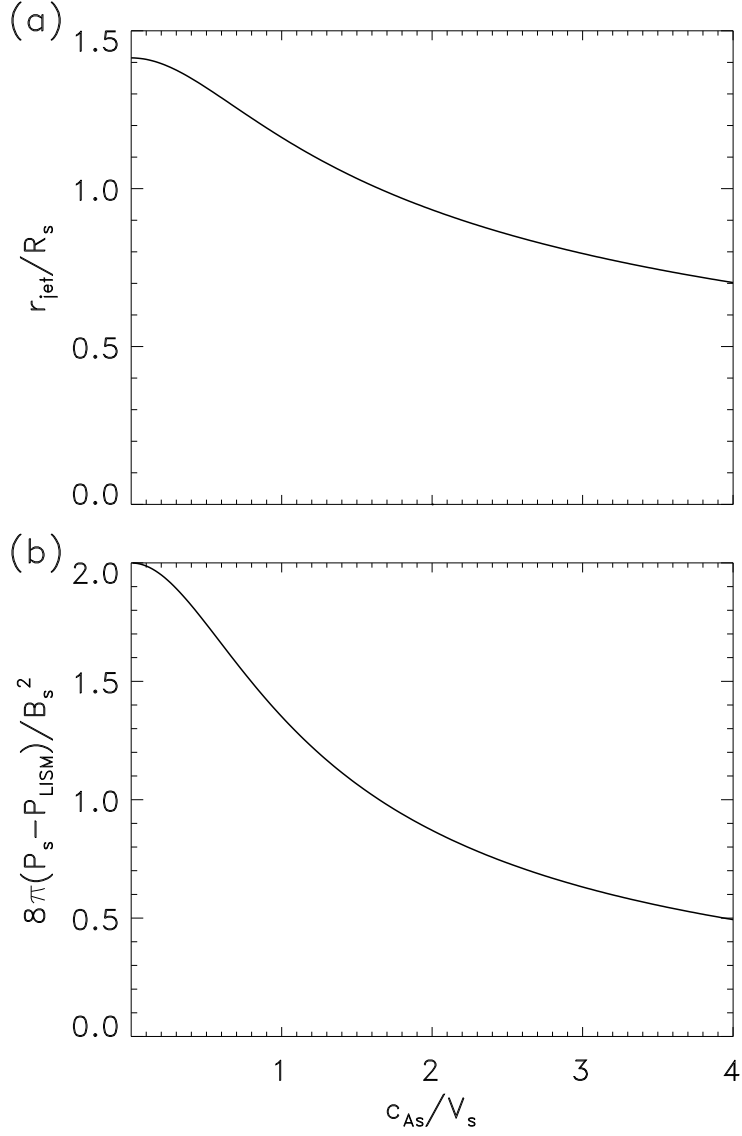


Fig. 3.— The jet radius r_{jet} and the pressure jump between the TS and interstellar medium, $P_s - P_{LISM}$, versus the Alfvén speed downstream of the TS at the equator, c_{As} .

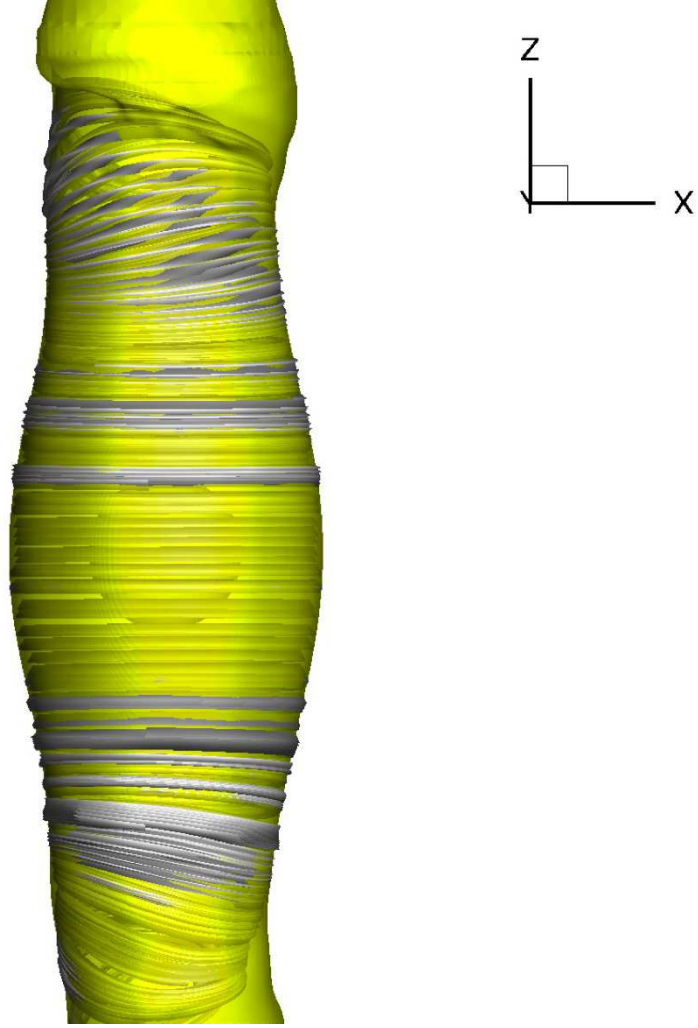


Fig. 4.— The heliopause as defined by $\ln T = 13.9$ from an MHD simulation embedded in an ambient interstellar medium with no mean flow and zero magnetic field. The gray lines are the solar magnetic field with the TS visible as a disc.

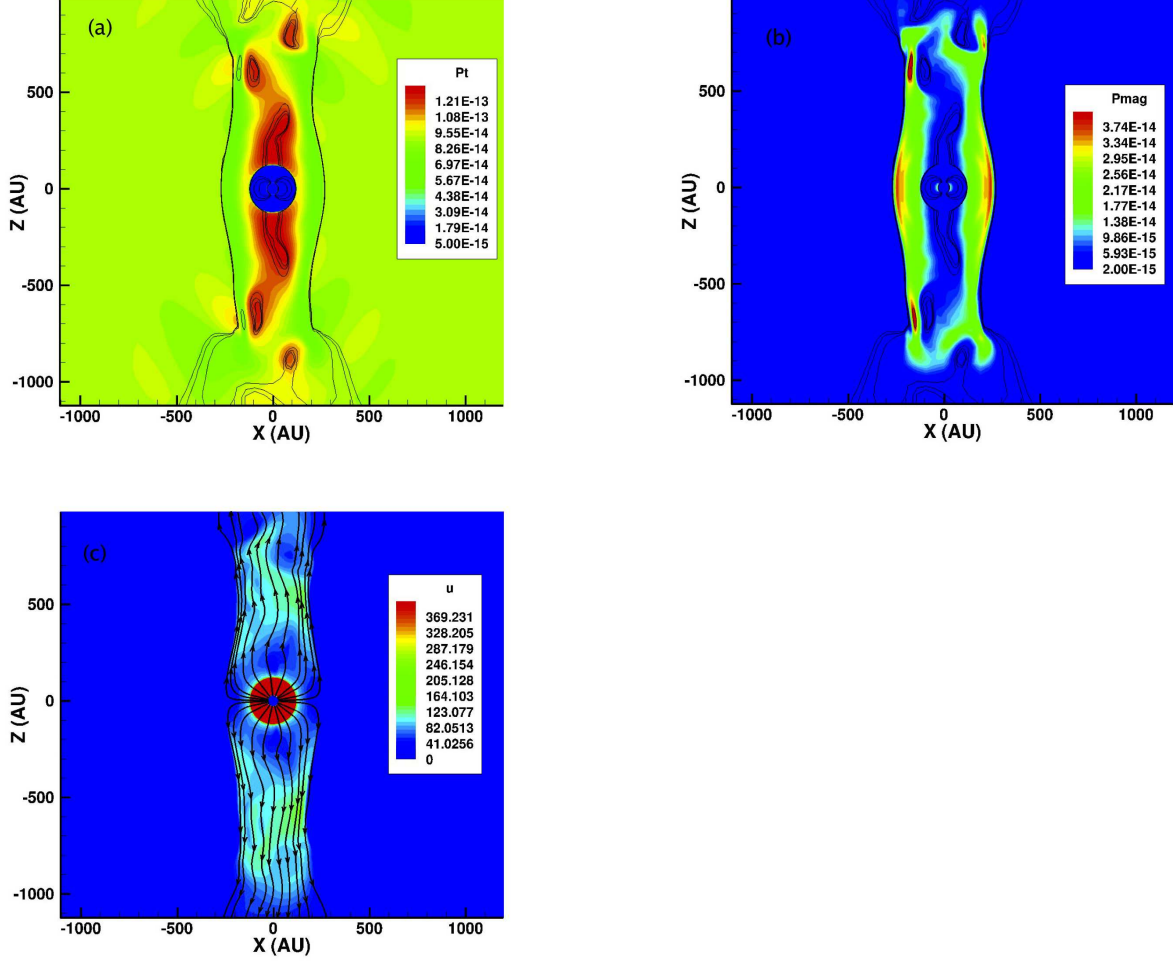


Fig. 5.— The plasma and magnetic pressures (Pa) in (a) and (b), and the plasma speed (km/s) and streamlines in (c). All in the $x - z$ plane through the center of the heliosphere from the simulation in Fig. 4.